

We are IntechOpen, the world's leading publisher of Open Access books Built by scientists, for scientists

6,900

Open access books available

186,000

International authors and editors

200M

Downloads

Our authors are among the

154

Countries delivered to

TOP 1%

most cited scientists

12.2%

Contributors from top 500 universities



WEB OF SCIENCE™

Selection of our books indexed in the Book Citation Index
in Web of Science™ Core Collection (BKCI)

Interested in publishing with us?
Contact book.department@intechopen.com

Numbers displayed above are based on latest data collected.
For more information visit www.intechopen.com



Interactions between Aquaporin Proteins and Block Copolymer Matrixes

Amira Abdelrasoul, Huu Doan and Ali Lohi

Additional information is available at the end of the chapter

<http://dx.doi.org/10.5772/intechopen.71723>

Abstract

This chapter continues to further expand its focus on aquaporins (AQPs) by offering a general outline on how the AQPs block copolymers, and polymer support structures can interrelate and such connections can be comprehensively classified and defined. The first section of the overview will consider the relationship between block copolymers and AQPs. It will also examine the general membrane protein integration into block copolymers, since this can cause AQP-block copolymer complexes in vesicular (proteopolymerosomes) as well as in planar forms. The majority of considerations taken into account during AQP incorporation come from the research conducted in relation to the process of incorporating other types of membrane proteins. This chapter includes an overview of the various characterization methodologies needed for the study of proteopolymerosomes, as well as freeze-fracture transmission electron microscopy (FF-TEM), fluorescence correlation spectroscopy (FCS), small-angle X-ray scattering (SAXS), and stopped-flow light scattering (SFLS). The research data presented in this chapter emphasizes the fact that a successful process of membrane fabrication requires the integration of reconstituted AQPs into a suitable supporting matrix formation.

Keywords: aquaporin proteins, block copolymer, matrix, vesicular, membrane protein

1. Assessing aquaporin proteins and block copolymer matrixes interactions

Most research performed on membrane protein inclusion has been conducted primarily with lipids as the host matrix components (original proteoliposomes publication on the subject came out in 1971) [1]. Since then, polymer-based incorporation process has received increased attention and the earliest proteopolymerosomes publication emerged in 2000 [2].

The initial work stages in this research area concentrated on the inclusion of membrane-spanning proteins, such as membrane-bound ion channels (ATPases) and bacteriorhodopsin incorporation into polymethyloxazoline-polydimethylsiloxane-polymethyloxazoline (PMOXA-PDMS-PMOXA) triblock copolymer bilayers occurring in planar [3] or vesicular forms [4–6]. It is quite fascinating that the membrane proteins may be functionally incorporated into polymeric bilayers (e.g., based on PMOXA-PDMS-PMOXA) that occur up to 10 times thicker than their lipidic counterparts [7]. Moreover, researchers have observed proteopolymersomes with protein density values that drastically surpassed those of proteoliposomes [8]. Research on these phenomena has helped to establish a theoretical approach for generalized membrane protein incorporation into the amphiphilic structures. This methodology is based on the notion that the efficiency of the membrane protein incorporation process relies on its hydrophobicity potential and its coupling capacity to the host membrane is directly connected to the hydrophobic mismatch parameters. In order to reduce this mismatch dynamic, the method calls for the host membrane to be deformed in such a way that it matches the hydrophobic length parameter of the membrane protein's trans-membrane segment, in this case the hydrophobic length is 3–4 nm. A different manner of adaption would produce alternative results since the host membrane-induced membrane protein deformation is improbable due to the fact that membrane protein compressibility potential is generally one or two orders of magnitude greater than the one present in lipids [9, 10]. Researchers Srinivas and Discher argue that the application of coarse-grain simulations can ensure that the flexible hydrophobic chains would allow protein incorporation. Srinivas and Discher add that this may occur even in cases where there is a hydrophobic mismatch greater than 22% between hydrophobic interior of the chain region and membrane proteins [11, 12]. As a consequence, membrane proteins may be included with greater efficacy if the hydrophobic chains are sufficiently flexible [10]. Stiffer chains that are more flexible can possibly block the channel, a distinct lack of proteopolymersomes functionality can be perceived, even though the membrane protein was functionally incorporated [11]. Furthermore, elevated polydispersity may facilitate higher incorporation efficiency levels, since smaller chains can collect around the membrane protein and then offset the hydrophobic mismatch potential. Sufficiently positive incorporation data detected in the case of PMOXA-PDMS-PMOXA can thus likewise be credited to the much higher polydispersity index (PDI). Alternatively, in the setting such as natural lipid environment, the natural lipids surrounding the incorporated protein may be chosen partially due to the similarity with the lateral diffusion and protein surface [13]. The collective consequences of the hydrophobic mismatch are substantial for ATPases, ion channels [9], and co-transporter proteins. On the other hand, the effects of the mismatch are noticeably less for AQPs where they are reduced, since the protein structure itself is intrinsically more rigid [14].

Stoenescu and coworkers conducted the initial incorporation of AQPs in polymer bilayer in 2004 [15]. A research team by Stoenescu included an AQP0 originating from the mammalian eye lens directly into the polymersomes of three diverse block architectures (ABA, ABC, CBA, with A standing in for PMOXA, B for PDMS, and C for polyethylene oxide, PEO). This type of block configuration shapes how the orientation of AQP0 is being incorporated will occur. The data results obtained in this case suggest that ABA featured 50%

of included AQP0 with an orientation comparable to the one occurring in liposomes, CBA included only 20%, while ABC had 80%, as shown in the antibody labeling. In all these test examples, the process of incorporation was accomplished using the addition of AQP0 content into the detergent during the polymersome configuration, as well as with the application of size exclusion chromatography (SEC) for the removal of non-incorporated protein content [15].

Kumar and coworkers were able to produce the first evidence and samples of functional AQP incorporation in 2007. Specifically, Kumar integrated bacterial AqpZ from *E.coli* in PMOXA-PDMS-PMOXA polymersomes [7] and then verified their overall functional capacity within the stopped-flow light scattering (SFLS). As a relatively familiar permeability characterization methodology, SFLS permits the shrinkage of polymersomes because of the response to osmolarity changes that are monitored for the duration of the process using light scattering. The integration of AqpZ facilitated an osmotic response of proteopolymersomes that is 800 times greater than the one occurring with empty polymersomes. This test case likewise indicated that the activation energy, that is the barrier for water passing through the AqpZ, was analogous to the one present in AQP reconstituted in frog oocytes and proteoliposomes. During the testing, the molar protein-to-amphiphile ratio (mPAR) for ideal AqpZ performance within the triblock copolymer system was determined to be 1:50, a ratio that correspond to a 1:100 in a (diblock or lipid) bilayer system scenario [7]. The elevated density reconstitution parameter of AQP is also demonstrated by the creation of 2D AQP crystals that help collect structural (crystallographic) information about AQP, a process similar to the one applied to lipid based 2D AQP crystals [16]. In this type of process, a monolayer of nickel-functionalized polybutadiene-polyethylene oxide (PB-PEO) is collected at the water-interface, and includes the presence of aqueous solution, histidine-tagged AqpZ, PDMS-PMOXA-PDMS, and mixed micelles of detergent [17]. The property of nickel affinity to histidine further connects the AqpZ to the PB-PEO layer [18], effectually creating a dynamic of AqpZ high packing within the layer. Once the detergent is removed with the aid of biobeads and the PB-PEO is taken out with imidazole, the closely packed AqpZ PMOXA-PDMS-PMOXA crystals remained; however, the left over amount was not sufficient for retrieving key structural data [19, 20]. Data suggest that 2D crystals may in fact be useful when it comes to researching the effects of AQP on polymer self-assembly for general types of applications. The AQP0 has been shown to easily form 2D crystals because of its natural properties, as it occurs in stack formations within the eye lens [21]. The essential data findings collected during this experiment suggest that the AQP0 shapes the self-assembling behavior of both polymers in way that it is reciprocal to the hydrophilic volume ratio f . As the mPAR values are increasing, the interfacial curvature becomes lower and the polymersomes form into membrane sheets as well as a certain amount of crystals (see **Figures 1** and **2**). When it comes to PB-PEO, the construction of polymersomes happened only when AQP0 was added, while in the absence of AQP0 solely cylindrical structures were perceived. The greatest packing densities of functional AQPs within vesicular structures were noted at PB-PEO polymersomes featuring an mPAR of 1:15, a correlation that is much higher than the one that was obtained in the cases with frog oocytes and proteoliposomes. While not all of the AQP0 proteins were integrated, this sevenfold growth in osmotic

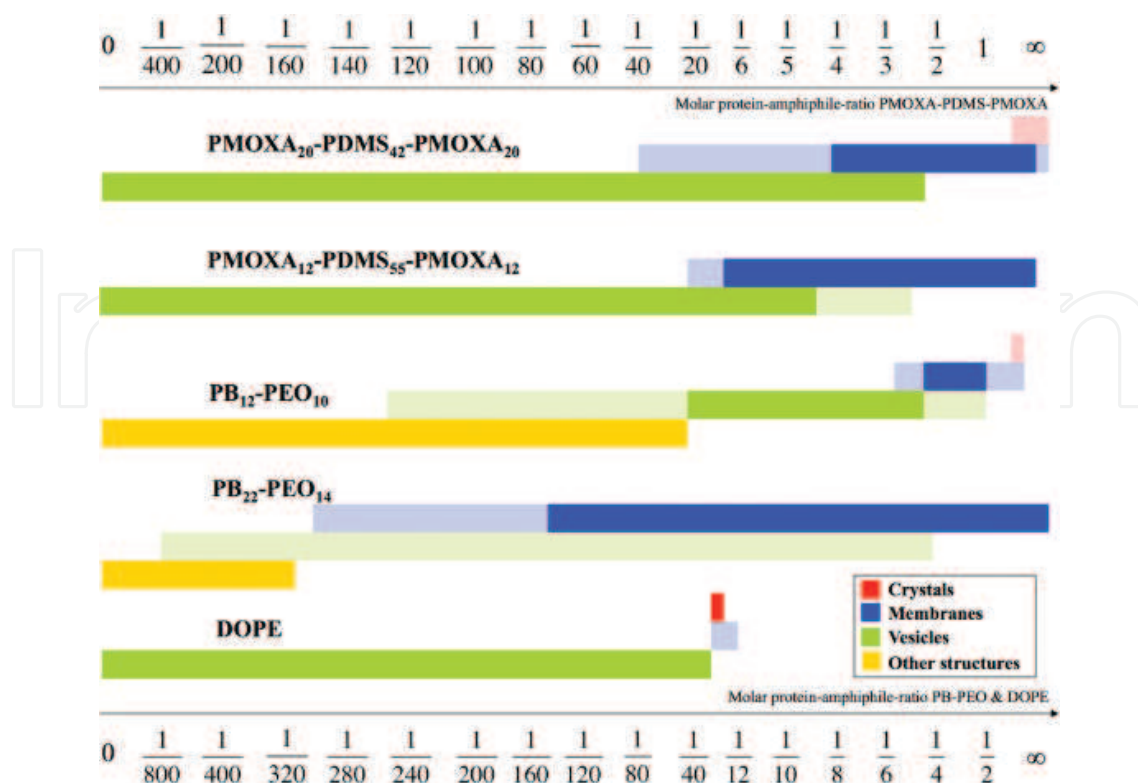


Figure 1. A schematic drawing of aggregate morphologies portrayed as a function of mPAR. PB12-PEO10 as it goes through four transitions. The morphologies shown in full color indicate the primary morphologies, where the pale colors signify the coexisting morphologies [24].

response values is relatively consistent with the high-packing density parameters and low permeability of AQP0 [22]. In this experimental run, the integration occurred through the process of mixing detergent-solubilized polymers with the detergent-solubilized AQP0, and then dialyzing the detergent out of the mixture [8, 23]. In this case, the vesicle's shape continued to show substantially greater densities at block copolymers, when correlated to standard types of lipids such as the 1,2-dioleoyl-sn-glycero-3-phosphoethanolamine (DOPE). The mPAR from the one-molecule bilayer-establishing ABA triblock copolymers was split by two, effectually allowing direct comparative analysis with the PB-PEO diblock copolymers and DOPE, both of which are acting as forming bilayers [24].

When it comes to the process of fabricating biomimetic membranes for a variety of applications, the original protein incorporation methodologies were from the period between 2009 and 2011 and were primarily based on the use of lipids [25, 26]. However, planar polymeric membranes have been effectively shown with the functional inclusion of gramicidin A [27]. Such research initiatives were first introduced by a Danish company called Aquaporin A/S. This company's innovative approaches to the process of biomimetic membrane fabrication will be examined in the later sections. This research will be supplemented with an overview of the data generated by the research groups working at the National University of Singapore (NUS) and the Singapore Membrane Technology Center (SMTC) at Nanyang Technological University (NTU).

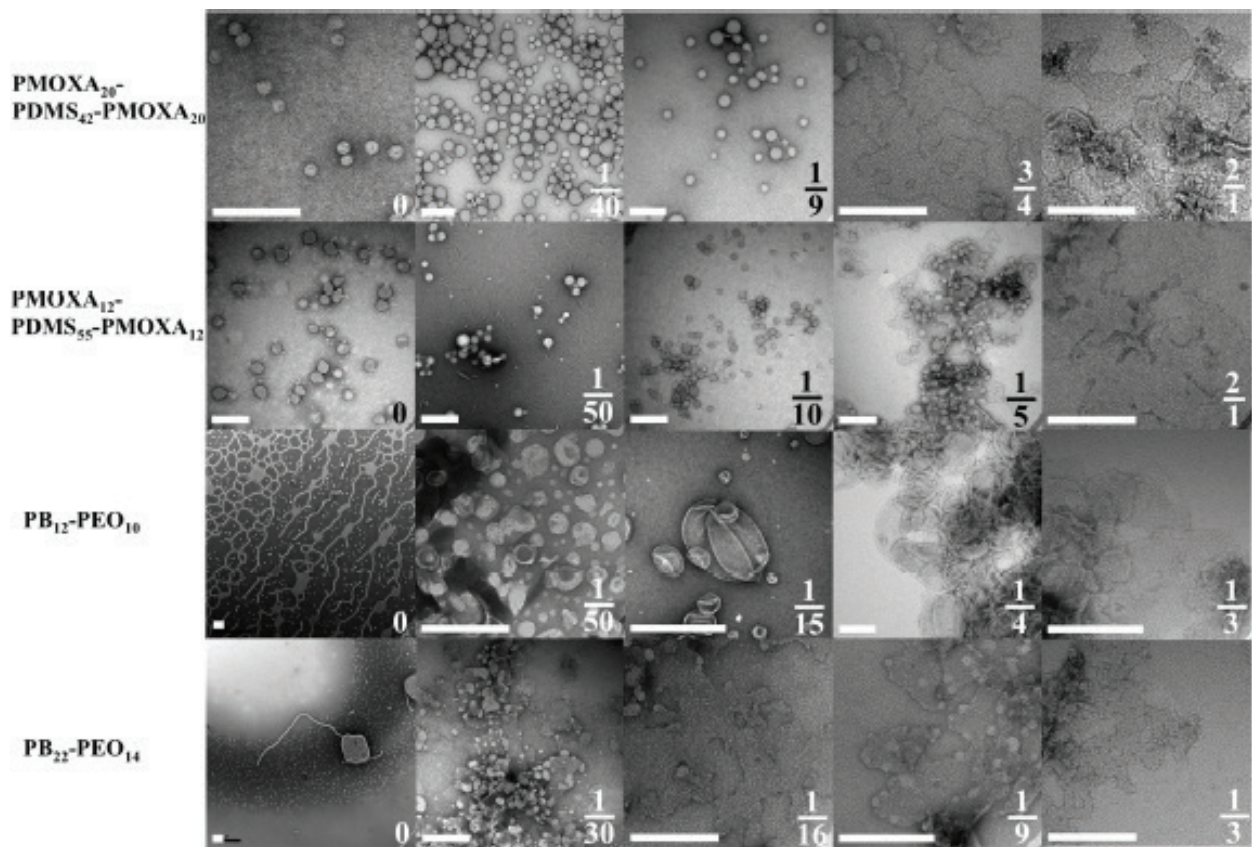


Figure 2. The TEM images of aggregate morphologies as a function of mPAR, where the PMOXA-PDMS-PMOXA copolymers self-assemble into vesicles, PB-PEO forms network- and sperm-like structures, however, only after incorporation of AQP0 vesicular structures are observed. Scale bar is 200 nm [23].

The overview in **Table 1** summarizes the critical research data on the experimental membrane protein and peptide, integration into block copolymer membranes. These data include information on a range of parameters, such as polymer chemistry and stoichiometry, *PDI*, the incorporated membrane protein, the number-average molecular weight (M_n), f , the transport cargo (e.g., water for AQP) if there was functional incorporation, mPAR values, how polymer and membrane protein were mixed, and the shape of the polymer self-assembled structure. The data also show how the function incorporation values were measured and how M_n (which can be quantified using NMR) is related to M_w as $PDI = M_w / M_n$. This table does not include the incorporation studies that do not include block copolymer-protein interactions, such as cell-free expression systems [73–75], nanopores [76, 77], encapsulation in hydrophobic interior [6], hydrogel approaches [78, 79], and non-amphiphilic polymers [80]. Due to this restriction on the data, the table showcases the results that were made available by Wolfgang Meier and coworkers implementing PMOXA-PDMS-PMOXA triblock copolymers.

An overview in **Figure 3** outlines data on membrane protein integration into polymers in cases where M_n and f are known. Every black dot signifies a single polymer. The connected box summarizes the data on incorporated membrane protein family, polymer chemistry,

Polymer	M_n	PDI	f	Membrane protein	Transport Cargo	FI	mPAR	S	Incorporation method	Main functional incorporation measurement	References
PMOXA ₁₃ - PDMS ₂₃ - PMOXA ₁₃	3.9				e ⁻	X	1:3300	V	MAq, biobeads, and SEC	Cargo → Reduction of MP → EPR signal	[28]
PMOXA ₁₃ - PDMS ₂₃ - PMOXA ₁₃	4.7	NA	0.44	Alamethicin		X	1:590	P	MAq	Current change	[29]
PMOXA ₁₃ - PDMS ₂₃ - PMOXA ₁₃	4.7	NA	0.44	Hemolysin		X	1:110,000,000	P	MAq	Current change	[29]
PMOXA ₁₃ - PDMS ₂₃ - PMOXA ₁₃	4.7	NA	0.44	OmpG		X	1:33,000,000	P	MAq	Current change	[29]
PMOXA ₂₀ - PDMS ₄₁ - PMOXA ₂₀	6.4	1.61	0.49	NtAQP1	CO ₂	X	1:360	P	MOr	Cargo → Reaction inside vesicle → pH change	[30]
PMOXA ₂₀ - PDMS ₄₁ - PMOXA ₂₀	6.4	1.61	0.49	NtPIP2:1	CO ₂	X	1:360	P	MOr	Cargo → Reaction inside vesicle → pH change	[30]
PMOXA ₂₀ - PDMS ₄₁ - PMOXA ₂₀	6.5	<1.2	0.51	AQP0	H ₂ O	ND	10:1–1:1	P	MAq and dialysis		[8]
PMOXA ₂₀ - PDMS ₄₁ - PMOXA ₂₀	6.5	<1.2	0.51	AQP0	H ₂ O	ND	10:1–1:50	V	MAq and dialysis		[8]
PMOXA ₂₀ - PDMS ₄₁ - PMOXA ₂₀	6.5	<1.2	0.51	AQP0	H ₂ O	—	1:2.5–0	V	MAq and dialysis	Vesicle size change	[8]
PMOXA ₁₂ - PDMS ₅₄ - PMOXA ₁₂	6.0	1.01	0.2	AqpZ	H ₂ O	X	1:100–1:1600	V	MAq and biobeads	Vesicle size change	[31]

Polymer	M _n	PDI	f	Membrane protein	Transport Cargo	FI	mPAR	S	Incorporation method	Main functional incorporation measurement	References
PMOXA ₁₉ - PDMS ₇₄ - PMOXA ₁₉	8.7	1.46	0.23								
PMOXA ₁₂ - PDMS ₅₄ - PMOXA ₁₂	6.0	1.01	0.3	AqpZ	H ₂ O	X	1:50–1:400	V	MAq and biobeads	Vesicle size change	[32, 33]
PMOXA ₁₂ - PDMS ₅₄ - PMOXA ₁₂	6.0	1.01	0.3	Hemolysin		–	1:83,000,000	P	MAq	Current change	[29]
PMOXA ₂₀ - PDMS ₅₄ - PMOXA ₂₀	7.4	NA	0.42	TsX	Nucleosides	X	1:450	V	MOr, SI, and SEC	Cargo → Encapsulated enzyme activity → Color change	[34]
PMOXA ₈ - PDMS ₅₅ - PMOXA ₈	5.4	NA	0.22	AqpZ	H ₂ O	X	1:3500	V	PFR, biobeads, and SEC	Vesicle size change	[35]
PMOXA ₁₂ - PDMS ₅₅ - PMOXA ₁₂	6.1	1.64	0.30	OmpF	ELF97	X	1:1200	V	MAq and SEC Cargo	Precipitation inside vesicle → Color change	[36]
PMOXA ₁₂ - PDMS ₅₅ - PMOXA ₁₂	6.1	1.64	0.30	OmpF	Acridine orange	X	1:9,100,000	V	PPFR and SEC	Cargo release → Color change	[37]
PMOXA ₁₂ - PDMS ₅₅ - PMOXA ₁₂	6.1	1.64	0.30	OmpF	Paraquat. Pyrocyanin	X	1:640	V	MAq and dialysis	No cargo → No detoxication of encapsulated enzyme → Cell death	[38, 39]
PMOXA ₁₂ - PDMS ₅₅ - PMOXA ₁₂	6.1	1.64	0.30	AQP0	H ₂ O	ND	10:1–1:25	P	MAq and dialysis		[8]
PMOXA ₁₂ - PDMS ₅₅ - PMOXA ₁₂	6.1	1.64	0.30	AQP0	H ₂ O	–	1:3–0	V	MAq and dialysis	Vesicle size change	[8]

Polymer	M_n	PDI	f	Membrane protein	Transport Cargo	FI	mPAR	S	Incorporation method	Main functional incorporation measurement	References
PMOXA ₁₂ - PDMS ₅₅ - PMOXA ₁₂	6.1	1.64	0.30	AqpZ	H ₂ O	ND	1:4	Cr,V	MAq and biobeads		[19]
PMOXA ₇ - PDMS ₆₀ - PMOXA ₇	5.6	NA	0.19	Gramicidin A	Monovalent cations	X	1:81,000	P	MOr	Current change	[27]
PMOXA ₈ - PDMS ₆₀ - PMOXA ₈	5.8	NA	0.21	ApqZ	H ₂ O	X	1:3800	V	PFR, biobeads, and SEC	Vesicle size change	[35]
PMOXA ₁₃ - PDMS ₆₂ - PMOXA ₁₃	6.8	1.47	0.29	NADH reductase	e ⁻	X	1:1900	V	MAq, biobeads, and SEC	Cargo → Reduction of MP → EPR signal	[28]
PMOXA ₁₅ - PDMS ₆₂ - PMOXA ₁₅	7.1	1.50	0.32	NADH reductase	e ⁻	X	1:1800	V	MAq, biobeads, and SEC	Cargo → Reduction of MP → EPR signal	[28]
PMOXA ₁₂ - PDMS ₆₅ - PMOXA ₁₂	6.9	1.67	0.27	MloK1	Potassium	X	1:390	P	MAq and biobeads	Current change	[40]
PMOXA ₁₅ - PDMS ₆₈ - PMOXA ₁₅	7.6	NA	0.30	LamB	Maltohexaose	X	NA	P	MAq	Current change at varying cargo concentrations	[41]
PMOXA ₁₅ - PDMS ₆₈ - PMOXA ₁₅	7.6	NA	0.30	OmpF	Acetylthiocholine	X	1:10,000	V	PFR	Cargo → Encapsulated enzyme activity → Color change	[41]
PMOXA ₁₅ - PDMS ₆₈ - PMOXA ₁₅	7.6	1.20	0.30	ApqZ	H ₂ O	X	1:10–1:1000	V	PFR and biobeads	Vesicle size change	[42]
PMOXA ₁₅ - PDMS ₆₈ - PMOXA ₁₅	7.6	1.20	0.30	Hemolysin			1:66,000,000	V	MAq	Current change	[29]

Polymer	M _n	PDI	f	Membrane protein	Transport Cargo	FI	mPAR	S	Incorporation method	Main functional incorporation measurement	References
PMOXA ₂₁ - PDMS ₆₉ - PMOXA ₂₁	8.7	2.00	0.37	NADH reductase	e ⁻	X	1:1500	V	MAq, biobeads, and SEC	Cargo → Reduction of MP → EPR signal	[28]
PMOXA ₁₆ - PDMS ₇₂ - PMOXA ₁₆	8.0	1.17	0.30	OmpF	Enone	X	1:220	V	PPFR and dialysis	Cargo → Encapsulated enzyme activity → Color change	[43]
PMOXA- PDMS- PMOXA	8.8	NA	NA	OmpF	ELF97	X	1:50	V	MAq and SEC	Cargo → Precipitation inside vesicle → Color change	[44]
PMOXA ₃₂ - PDMS ₇₂ - PMOXA ₃₂	10.7	1.83	0.47	OmpF	7-ADCA, PGME	X	NA	V	PFR and dialysis	Cargo → Encapsulated enzyme activity → Bacterial death	[45]
PMOXA ₁₁ - PDMS ₇₃ - PMOXA ₁₁	7.2	1.70	0.22	LamB	DNA	X	1:390	V	MOr, SI, and SEC	Fluorescence – labeled cargo	[46]
PMOXA ₁₁ - PDMS ₇₃ - PMOXA ₁₁	7.2	1.70	0.22	OmpF	Nucleosides	X	1:10–1:100	V	PPFR and SEC	Cargo → Encapsulated enzyme activity → Color change	[47]
PMOXA ₁₁ - PDMS ₇₃ - PMOXA ₁₁	7.2	1.70	0.22	TsX	Nucleosides	X	1:10–1:100	V	PPFR and SEC	Cargo → Encapsulated enzyme activity → Color change	[47]
PMOXA ₁₁ - PDMS ₇₃ - PMOXA ₁₁	7.2	1.70	0.22	LamB	DNA	X	NA	P	MAq		[46]
Lipids											
PMOXA ₂₁ - PDMS ₇₃ - PMOXA ₂₁	9.0	1.70	0.36	Alamethicin	Calcium	X	1:24	V	MAq	Cargo precipitation inside vesicle	[48, 49]

Polymer	M_n	PDI	f	Membrane protein	Transport Cargo	FI	mPAR	S	Incorporation method	Main functional incorporation measurement	References
PMOXA ₂₁ - PDMS ₇₃ - PMOXA ₂₁	9.0	1.70	0.36	FhuA	Sulphorhodamine B	X	1:6,000,000	V	MOr, SI, and SEC	Cargo → Quenching inside vesicle → Color change	[50–52]
PMOXA ₂₁ - PDMS ₇₃ - PMOXA ₂₁	9.0	1.70	0.36	FhuA	TMB	X	1:4500. 1:3,600,000	V	MAq/ and biobeads/MOr, SI, and SEC	Cargo → Encapsulated enzyme activity → Color change	[50, 51, 53]
PMOXA ₂₁ - PDMS ₇₃ - PMOXA ₂₁	9.0	1.70	0.36	FhuA		ND	3000:1	P	MAq		[51]
PMOXA ₂₁ - PDMS ₇₃ - PMOXA ₂₁	9.0	1.70	0.36	FhuA	NAD	—	NA	V	MAq	Cargo → Encapsulated enzyme activity → Absorbance change of cargo	[52]
PMOXA ₂₁ - PDMS ₇₃ - PMOXA ₂₁	9.0	1.70	0.36	FhuA	DNA	—	NA	V	MOr, SI, and SEC	Fluorescence-labeled cargo	[52]
PMOXA ₂₁ - PDMS ₇₃ - PMOXA ₂₁	9.0	1.70	0.36	LamB	Sugar	X	NA	P	MAq	Current change at varying cargo concentration	[54]
PMOXA ₂₁ - PDMS ₇₃ - PMOXA ₂₁	9.0	1.70	0.36	OmpF	e ⁻	X	NA	P	MAq	Current change	[54]
PMOXA ₂₁ - PDMS ₇₃ - PMOXA ₂₁	9.0	1.70	0.36	OmpF	Ampicillin	X	1:1000	V	MOr and SEC	Cargo → Hydrolysis inside vesicle → Color change	[12, 55]
PMOXA ₂₀ - PDMS ₇₅ - PMOXA ₂₀	9.0	1.46	0.34	AqpZ	H ₂ O	X	1:25, 1:50, 1:200	V	PFR and biobeads	Vesicle size change	[56]
PMOXA ₁₁ - PDMS ₇₆ - PMOXA ₁₁	7.8	1.48	0.25	BR	H ⁺	X	NA	V/Mc	MOr and SI	pH change	[57, 58]

Polymer	M _n	PDI	f	Membrane protein	Transport Cargo	FI	mPAR	S	Incorporation method	Main functional incorporation measurement	References
PMOXA ₁₁ - PDMS ₇₆ - PMOXA ₁₁	7.8	1.48	0.25	BR and ATPase	H ⁺	X	1:180	V	MOr and dialysis	pH change and bioluminescence assay	[15]
PMOXA ₁₁ - PDMS ₇₆ - PMOXA ₁₁	7.8	1.48	0.25	BR and ATPase	H ⁺	X	1:20	V	PBR and dialysis	pH change	[59–61]
PMOXA ₆ - PDMS ₉₀ - PMOXA ₆	9.5	NA	0.12	OmpF	L-ascorbic acid, CO, Na ₂ S ₂ O ₄ , ONOO ⁻	X	1:1300	V	PFR, dialysis, and SEC	Cargo → Absorbance change of encapsulated protein	[62]
PMOXA ₂₁ - PDMS ₉₇ - PMOXA ₂₃	9.0	1.70	0.30	Hemagglutinin		X	1:3800	V	MAq and biobeads	MP → Fusion with fluorescence-labeled liposomes	[53]
PMOXA ₉ - PDMS ₁₀₆ - PMOXA ₉	9.4	1.38	0.14	NADH reductase	e ⁻	X	1:1400	V	MAq, biobeads, and SEC	Cargo → Reduction of MP → EPR signal	[38]
PMOXA ₁₃ - PDMS ₁₁₀ - PMOXA ₁₃	10.4	1.44	0.19	NADH reductase	e ⁻	X	1:1200	V	MAq, biobeads, and SEC	Cargo → Reduction of MP → EPR signal	[38]
PMOXA ₁₄ - PDMS ₁₁₀ - PMOXA ₁₄	10.4	1.36	0.20	NADH reductase	e ⁻	X	1:1200	V	MAq, biobeads, and SEC	Cargo → Reduction of MP → EPR signal	[38]
PMOXA ₁₅ - PDMS ₁₁₀ - PMOXA ₁₅	10.7	1.62	0.21	AqpZ	H ₂ O	X	1:25–1:500	V	PFR and SEC	Vesicle size change	[7, 19]
PMOXA ₁₅ - PDMS ₁₁₀ - PMOXA ₁₅	10.7	1.62	0.21	OmpF		ND	NA	P	MAq		[53]
PMOXA- PDMS- PMOXA	20.0	NA		FhuA	Calcein	X	1:2,700,000	V	MOr, SI, and SEC	Cargo release → Color change	[54]

Polymer	M _n	PDI	f	Membrane protein	Transport Cargo	FI	mPAR	S	Incorporation method	Main functional incorporation measurement	References
PMOXA ₆₅ - PDMS ₁₆₅ - PMOXA ₆₅		23.3	1.63	NADH reductase	e ⁻	X	1:550	V	MAq, biobeads, and SEC	Cargo release → Reduction of MP → EPR signal	[28]
PMOXA- PDMS- PMOXA	NA	NA	NA	BR	H ⁺	X	NA	P	MAq	pH change	[55, 56]
PMOXA- PDMS- PMOXA	NA	NA	NA	BR and CcO	H ⁺ and e ⁻	X	NA	V	MOr, SI, and SEC	Current and pH change	[56, 57]
PMOXA- PDMS- PMOXA	NA	NA	NA	CcO	e ⁻	X	NA	P	MOr, SI, and SEC	Current change	[55, 56]
PMOXA- PDMS- PMOXA	NA	NA	NA	OmpF	H ⁺	X	NA	P	MAq	Current change	[58]
PMOXA ₁₁₀ - PDMS ₄₀ - PEO ₂₅	13.4	NA	0.75	AQP0	H ₂ O	ND	1:200	V	MOr, SI, and SEC		[15]
PMOXA ₄₅ - PDMS ₄₀ - PMOXA ₆₇	10.6	NA	0.68	AQP0	H ₂ O	ND	1:200	V	MOr, SI, and SEC		[15]
MPEG-PVL	6.5	<1.2	0.00	Polymyxin B	Calcein	X	1:2	V	MAq	Cargo release → Color change	[63]
P2VP-PEO	NA	NA	NA	FhuA	NAD	—	NA	V	MOr, SI, and SEC	Cargo → Enzyme reaction inside vesicle → Absorbance change of cargo	[63]
PB ₁₂ -PEO ₁₀	1.1	1.09	0.32	AQP0	H ₂ O	X	1:5–1:250	V	MAq and dialysis	Vesicle size change	[8]
PB ₁₂ -PEO ₁₀	1.1	1.09	0.32	AQP0	H ₂ O	ND	1:1.3	Cr	MAq and dialysis		[8]
PB ₁₂ -PEO ₁₀	1.1	1.09	0.32	AQP0	H ₂ O	ND	1:1–1:10	P	MAq and dialysis		[8]
PB ₁₂ -PEO ₁₀	1.1	1.09	0.3	AqpZ	H ₂ O	X	1:50–1:1000	V	MAq and dialysis	Vesicle size change	[59]

Polymer	M _n	PDI	f	Membrane protein	Transport Cargo	FI	mPAR	S	Incorporation method	Main functional incorporation measurement	References
PB ₁₂ -PEO ₁₀	1.1	1.09	0.32	BR	H ⁺	X	1:500	V	MAq and biobeads	pH change	[60]
PB ₁₂ -PEO ₁₀	1.1	1.09	0.3	SoPIP2;1	H ₂ O	—	1:200	V	MAq and biobeads	Vesicle size change	[59]
PB ₁₂ -PEO ₁₀	1.1	NA	0.34	Hemolysin	Calcein	X	1:33,000	V	MAq and dialysis	Cargo release → Color change	[61]
PB ₂₂ -PEO ₁₄	1.8	1.17	0.28	AQP0	H ₂ O	ND	2:1–1:300	P	MAq and dialysis		[8]
PB ₂₂ -PEO ₂₃	2.2	1.09	0.39	AqpZ	H ₂ O	X	1:15–1:200	V	MAq and dialysis	Vesicle size change	[59]
PB ₂₂ -PEO ₂₃	2.2	1.09	0.39	SoPIP2;1	H ₂ O	—	1:15–1:200	V	MAq and dialysis	Vesicle size change	[59]
PB ₂₉ -PEO ₁₆	2.3	1.00	0.25	AQP10	H ₂ O	—	1:990	V	PFR and SE	Vesicle size change	—
PB ₃₅ -PEO ₁₄	2.5	1.09	0.19	AqpZ	H ₂ O	—	1:15	V	MAq and dialysis	Vesicle size change	[59]
PB ₃₅ -PEO ₁₄	2.5	1.09	0.19	SoPIP2;1	H ₂ O	—	1:15	V	MAq and dialysis	Vesicle size change	[59]
PB ₄₃ -PEO ₃₂	3.7	1.03	0.31	AQP0	H ₂ O	X	1:600	V	PFR and SE	Vesicle size change	[62]
PB ₄₆ -PEO ₃₀	3.8	1.04	0.28	AqpZ	H ₂ O	—	1:50, 1:100, 1:200	V	MAq and dialysis	Vesicle size change	[59]
PB ₄₆ -PEO ₃₂	3.9	1.00	0.30	AQP0	H ₂ O	—	1:580	V	PFR and SE	Vesicle size change	—
PB52-PEO29	4.1	<1.1	0.25	Hemolysin	e ⁻	X	NA	P	MAq	Current change	[64]
PB52-PEO29	4.1	<1.1	0.25	Polymyxin B		X	NA	P	MAq	Current change	[65]
PB52-PEO29-LA	4.1	<1.1	0.25	Hemolysin	e ⁻	X	NA	P	MAq	Current change	[64]
PB52-PEO29-LA	4.1	<1.1	0.25	Polymyxin B		X	NA	P	MAq	Current change	[65]
PB92-PEO78	8.4	1.08	0.34	AQP0	H ₂ O	—	1:270	V	PFR and SE	Vesicle size change	—
PB125-PEO80	8.9	<1.1	0.28	Alamethicin	Calcein	—	1:2–1:8	V	MAq	Cargo release → Color change	[66]

Polymer	M _n	PDI	f	Membrane protein	Transport Cargo	FI	mPAR	S	Incorporation method	Main functional incorporation measurement	References
PHEMA25-PBMA25-PHEMA25	14.3	1.30	0.83	AqpZ		—	NA	P	MAq and biobeads	Current change	[67]
PHEMA25-PBMA25-PHEMA25	14.3	1.30	0.83	Hemolysin		X	NA	P	MAq	Current change	[67]
PHEMA25-PBMA25-PHEMA25	14.3	1.30	0.83	OmpF		—	1:70	P	MAq and biobeads	Current change	[67]
PEE37-PEO40	3.9	<1.1	0.39	Alamethicin	Calcein	X	1:2–1:8	V	MAq	Cargo release → Color change	[66]
PPO34-PGM14	6.5	1.30	0.66	Streptavidin-BSA		ND	1:5, 1:15, 1:50	V	PPFR		[68]
PI93-PEO87	10.2	1.00	0.31	FhuA	TMB	X	1:6700, 1:5,300,000	V	MOr, SI, and SEC	Cargo → Encapsulated enzyme activity → Color change	[63]
PEO136-PIB18-PEO136	8.0	1.86	0.90	Cecropin A	Calcein	X	1:30	V	MAq and SEC	Cargo release → Color change	[69]
P4MVP21-PS26-P4MVP21	13.1	NA	0.80	PR		X	1:10	V	MAq and precipitation	Absorbance change in membrane protein	[70]
P4MVP21-PS38-P4MVP21	14.3	1.19	0.74	PR		X	1:10	V	MAq and precipitation	Absorbance change in membrane protein	[70]
P4MVP29-PS42-P4MVP29	18.7	NA	0.78	PR		X	1:10	V	MAq and precipitation	Absorbance change in membrane protein	[70]
P4MVP22-PB28-P4MVP22	15.0	NA	0.92	PR		ND	1:10	V	MAq and precipitation		[71]

Polymer	M _n	PDI	f	Membrane protein	Transport Cargo	FI	mPAR	S	Incorporation method	Main functional incorporation measurement	References
P4MVP22-PB28-P4MVP22	15.0	NA	0.92	RC	e ⁻	X	1:25	V	MAq and precipitation	Cargo → Reduction of MP → EPR signal	[72]
P4VP22-PB28-P4VP22	7.1	NA	0.82	PR		ND	1:10	V	MAq and precipitation		[71]
P4MVP29-PB56-P4MVP29	17.4	1.08	0.81	RC	e ⁻	X	1:25	V	MAq and precipitation	Cargo → Reduction of MP → EPR signal	[72]
P4MVP18-PB93-P4MVP18	13.9	1.06	0.62	PR		ND	1:10	V	MAq and precipitation		[71]

Table 1. Overview of studies of membrane protein incorporation into amphiphilic block copolymers. Most studies are done with the porin OmpF, followed by AqpZ.

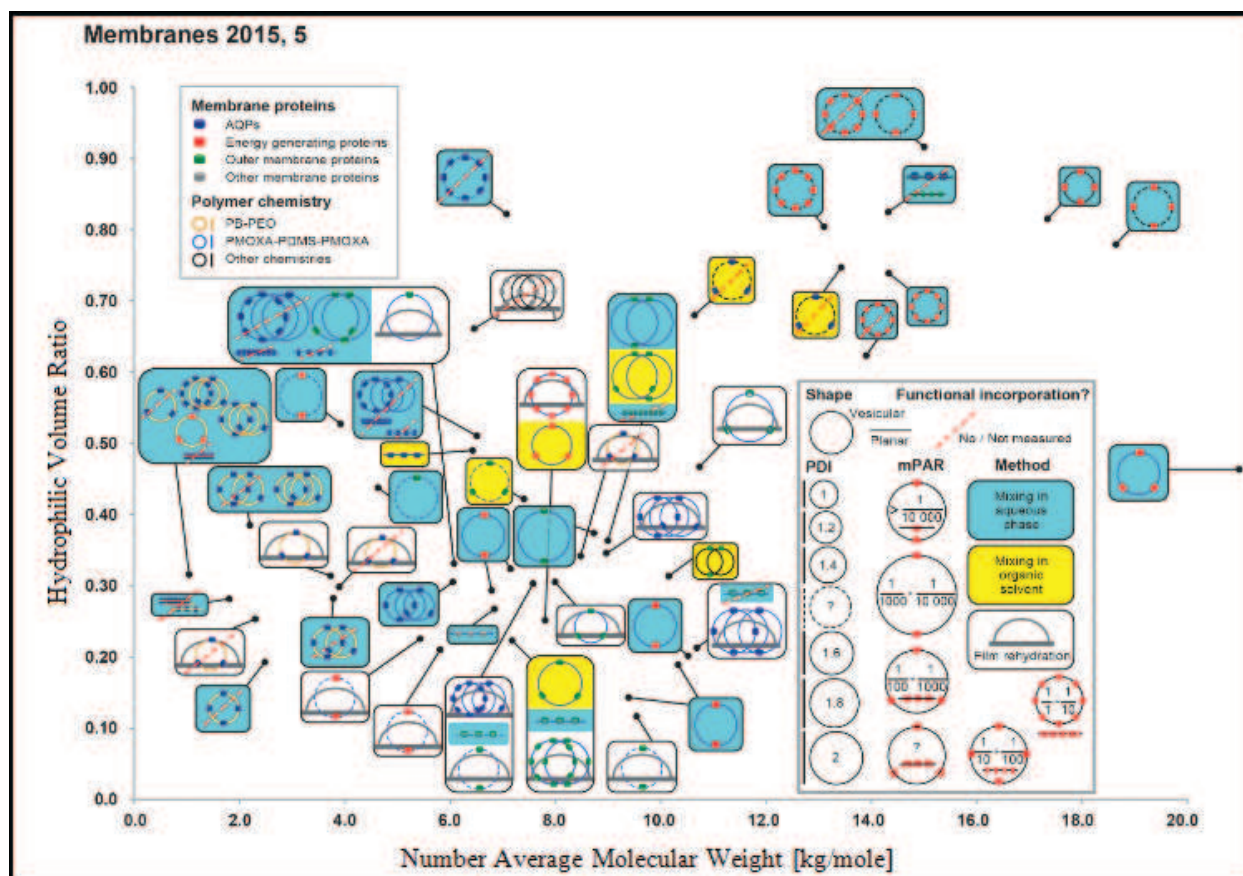


Figure 3. Summary of key parameters for membrane protein inclusion into amphiphilic block copolymers [81].

self-assembled morphology either planar or vesicular, *PDI* value of the polymer (rather than of the polymersomes), *mPAR* value, incorporation methodology, and if the incorporation process was functional, dysfunctional, or otherwise not measured. In instances where there are multiple sketches available in the box, then a variety of experimental runs have been conducted on the specific polymer example. Two crossing circles and two close lines, respectively, indicate that two different *mPAR*s were researched under the same maintained circumstances. A dynamic with three crossing circles designates that three *mPAR*s or more were examined. Whenever a parameter other than *mPAR* is investigated, such as incorporation method, incorporated membrane protein, or polymer chemistry, there is a new sketch available. In most cases, polymers that can engage in the process of functional incorporation require an *f* value somewhere between 0.2 and 0.35, and M_n value in the range of 2 and 12 kg/mol. In comparison to PB-PEO, PMOXA-PDMS-PMOXA has a significantly broader *PDI* [81] range, since its bilayer is water impermeable [7] and generally does not collapse in its dried form [82]. On the other hand, PB-PEO is noticeably more lipid-like because of its capacity to collapse easier and its greater water permeability potential [8]. Research suggests that these polymers that could not attain functional AQP incorporation are mostly PB-PEO polymers featuring small M_n and *PDI* values. The energy generating proteins (BR, CcO, NADH reductase, ATPase, RC, PR) and outer membrane proteins (OmpF, OmpG, FhuA, TsX) were integrated primarily into

PMOXA-PDMS-PMOXA polymers. However, the outer membrane proteins have likewise been integrated into somewhat more exotic chemistries occurring in an f range where there is no expectation to locate vesicular structures. The vast majority of the experimental trials on functional incorporation were conducted with vesicular structures and with the mixing processes occurring in aqueous phase. In fact, most experimental cases at smaller *PDI* parameters showed that no functional membrane proteins could be integrated. This particular dynamic is in agreement with the research data released by Pata et al. [10]. Various types of mPARs have been actively implemented, only to arrive at the fact that no optimal ratios can be identified. Nevertheless, mPARs are grounded on the nominal or initial concentration values of polymers and membrane proteins, where the final mPAR data after the incorporation is completed may vary [83]. The section to follow will examine a number of approaches to quantifying membrane proteins, with particular focus on AQPs, and after the overview of the incorporation process.

2. Evaluation of AQP incorporation characterization methodologies

The process of identifying examples of functional AQPs incorporation may strike as potentially quite challenging, since the permeating solute is composed of neutral water molecules. The protein-mediated type of transport when it comes to neutral molecules, and specifically at the single protein levels, is consistently more difficult to assess than the transport parameters of charged molecules, such as ions or protons or in cases of specific chemical reactions, including the ATPase enzyme activity. While the deuterated water labeling was suggested as a measurement method using the Raman spectroscopy [84], researchers are concerned that these approaches to measurement can be further complicated because the water transport rate value in the AQP channel varies for deuterated water molecules when compared to the normalized water molecule rate [85]. SFLS is a common methodology used for calculating the functional integration. SFLS method relies on a dynamic where the proteopolymersomes are vigorously combined with an osmotically active agent (NaCl or sucrose) within a specifically defined amount of volume. If a hyperosmotic shock occurs, the proteopolymersomes will become smaller in size and this in turn will facilitate light scattering to increase. Once the content of incorporated AQPs is augmented, the overall shrinking rate will likewise begin to increase. Nonetheless, the SFLS approach is substantially influenced by the quality, or size distribution potential, of the polymersomes, the concentration of the osmolytes, and the AQP concentration within the polymersomes [35]. In theory, a visually based measurement can be accomplished using the freeze-fracture transmission electron microscopy (FF-TEM), however, the FF-TEM will not be able to provide sufficient data on the functional aspects. During the FF-TEM assessment, the proteopolymersomes are caught in their original shape with the aid of the quick-freezing process. After the proteopolymersomes are collected, the frozen sample is then fractured in such a manner that the fracture plane is located alongside the proteopolymersome bilayer, since this section is the most vulnerable point in the entire system. The experimental samples with integrated AQPs, or the cavities in which the AQPs were inserted within the bilayer, are subsequently exposed to the carbon/metal coating process. The replica

formed during this procedure is then detached from the thawed out sample. As a result, the AQPs and cavities can be viewed and examined on the formed replica in the shape of separate spots on the proteopolymersomes content.

Alternative methodology available is the fluorescence correlation spectroscopy (FCS) process of the fluorescently labeled AQP. The FCS is based on the time-dependent fluctuations of fluorescence intensities within a defined microscopic space, otherwise known as the confocal volume, which are carefully observed and then exposed to autocorrelation function process. The specific number of particles within the confocal volume at given time interval can be calculated, however it depends on the diffusion times of particles spreading through the confocal volume. After the proper proteopolymersomes or proteoliposomes monitoring process, they are solubilized to micelles and monitored once more so as to calculate the proteins-per-vesicle-ratio, or the primary number of membrane proteins integrated into the bilayer of a single vesicle. Within this experimental scenario, it is presupposed that the micelles include only one AQP, and as a result the micelle-per-vesicle ratio is equivalent to the proteins-per-vesicle-ratio value. Additional information on the methodology is provided in Ref. [83]. On the other hand, it is possible to calculate the proteins-per-vesicle-ratio using a correlation between the proteopolymersome solution data and the AQP stock solution parameters.

In both of the outlined methodologies, the overall correlations of data have certain benefits as well as challenges, and these are outlined in greater detail in the FCS subsection. Small-angle X-ray scattering (SAXS) capacity to characterize the biological materials makes it an adaptive toolkit when it comes to particle structure. For instance, it can supply structural data about particles in a solution on a long-scale from 1 to 100 nm, and where the collected data is shown using scattering intensity values as a function of the magnitude parameter of the scattering vector q . The identified quantity is not dependent on experimental set-up's particular geometry and is linked directly to the scattering angle 2θ as $q = 4\pi \sin(\theta)/\lambda$, where λ is the wavelength value of the X-ray beam. The two scattering points that are separated by a distance d within a particle lead to an interference change that is signified by the scattering curve's increased intensity at $q = 2\pi/d$. The change in values implies that the larger sized features are probed at low q values and the smaller sized details are probed in the high- q region of the observed curves. Both the contrast and the strength with which a particle scatters is directly proportional to the particle's excess electron density, that is, the differentiation between the solvent used and the sample's electron density values. One of the SAXS issues is that this method demands access to extensive synchrotron radiation sources.

The upcoming section is an overview of SFLS, FF-TEM, FCS, and SAXS analyses featuring a variety of diblock copolymers containing optimal M_n and f range values for functional membrane protein integration processes, including PB29-PEO16, PB45-PEO14, PB33-PEO18, PB46-PEO32, PB92-PEO78, and PB43-PEO32. The PB-PEO was selected due to its functional AQP incorporation potential as reviewed earlier and the M_n and f range values that are simpler to manage in comparison to those of PMOXA-PDMS-PMOXA. For SFLS,

SAXS, and FF-TEM, the AqpZ is applied as the integrated membrane protein, while the GFP-tagged human aquaglyceroporin AQP10 is used as part of the FCS experimental runs. The data relevant to these types of incorporation are listed in the supplemental material.

2.1. Stopped-flow light scattering

An illustration of the SFLS and its analysis, the information about PB45-PEO14 and PB33-PEO18 diblock copolymer proteo- and polymersomes, specifically with or without AqpZ, is outlined in **Figure 4**. In the case of PB33-PEO18, the rate constant value related to the augmentation of the light scattering intensity was somewhat greater when using AqpZ, while for PB45-PEO14, the rate it was even smaller. Such a dynamic demonstrates one of the major issues that exist with respect to the SFLS application. The distinct lack of substantial response to the alterations in extra vesicular osmolarity can be caused by the growth in the bilayer bending modulus caused by the existence of AqpZ, either blocked or non-functional. Analogous concerns have been noted in previous experimental runs using AqpZ as well as SoPIP2, and where only polymers of the smallest size (PB12-PEO10 and PB22-PEO23) showed a considerable change in SFLS between proteo- and polymersomes (the results are not shown). Additional explanation for the analogous SFLS signal could be found in the blockage of AqpZ channels with PEO chains. In this type of blockage, the AqpZ are situated directly in the bilayer and act as an impermeable hydrophobic blockage. Research conducted by Kumar et al. [8] indicates that this blockage dynamic is caused by the water permeation that is actively blocked by the sections corresponding to the integrated AqpZ, and where the proteopolymersomes' lower permeability values can be expected, if compared to the values

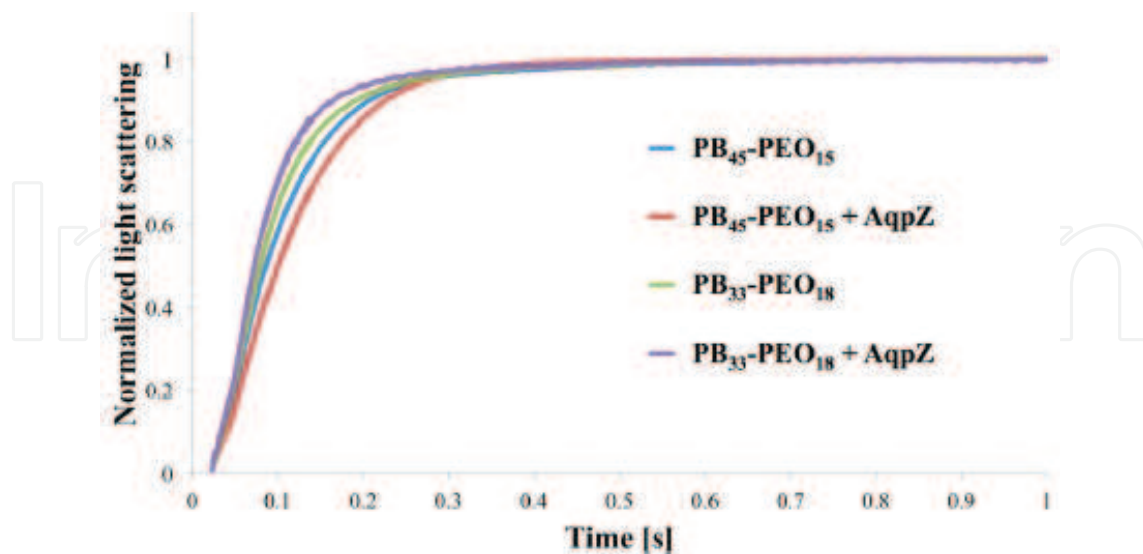


Figure 4. Normalized light scattering versus time for proteo- and polymersomes of PB45-PEO14 and PB33-PEO18, at an mPAR of 1:100. For PB45-PEO14 the apparent water permeability value is slightly lower for the proteopolymersomes *versus* polymersomes, while for PB33-PEO18 it is slightly increased [8].

occurring when using polymersomes. Alternatively, the incorporated AqpZ may continue being fully functional, while the polymer matrix remains resistant to various changes in volume parameters. These phenomena effectually undermine the idea that SFLS is not a stand-alone type of technique.

2.2. Freeze-fracture transmission electron microscopy

The summary of research data on FF-TEM for PB45-PEO14 proteopolymersomes is shown in **Figure 5**. Specifically, proteopolymersomes featuring an mPAR of 1:100 were created with the help of film rehydration (FR) approach, where they are frozen and then fractured in a Leica MED20 station. In the next step, the two planchets of the frozen sample are carefully separated, causing an intentional fracture that simulates something like a “crack” rather than a “cut” shape, which in turn lowers the smearing effects from the conventional FF procedures (for additional details refer to relevant supporting information). It is likely that because of the collapsed PB chains, all proteo- and polymersomes featured a distinguishable surface similar to a raspberry. In fact, the “typically” present spots that studies on proteoliposomes are usually associating with AQP [86] were not found. **Figure 5** outlines the bubble-like spots and their equal distribution among the polymersomes (**Figure 5a–d**) and proteopolymersomes (**b, c, e, f**). These bubble resembling spots may be PB chain accumulations (**Figure 5a–c**), or alternatively, phenomena produced by inferior fracturing (d–f) quality. Similar behavior was seen in proteo- and polymersomes in other PB-PEO polymers at different M_n and f values. The results collected during these experiments seem to indicate that FF-TEM sample preparation

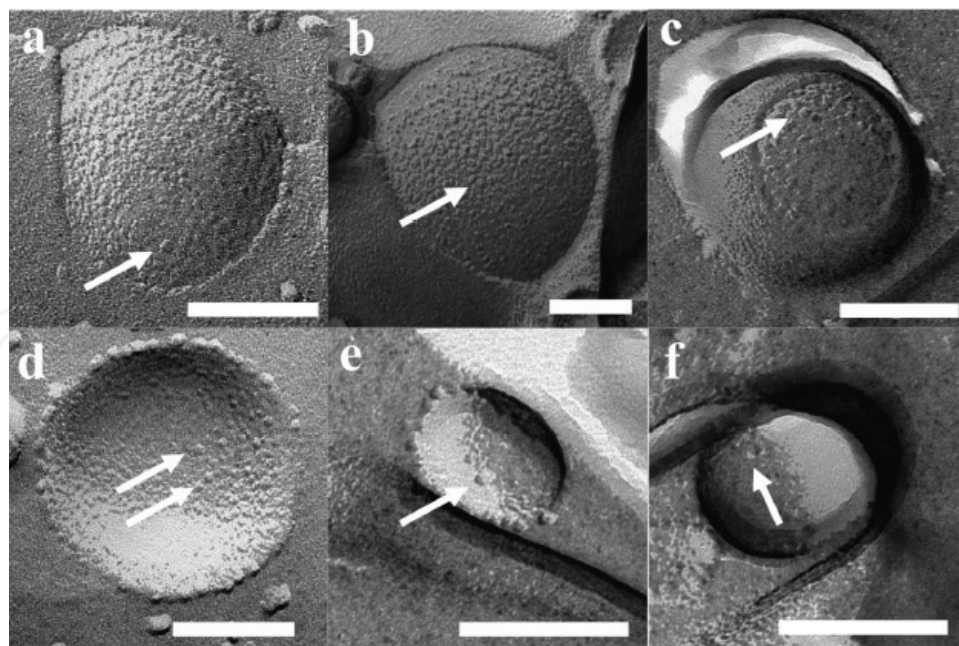
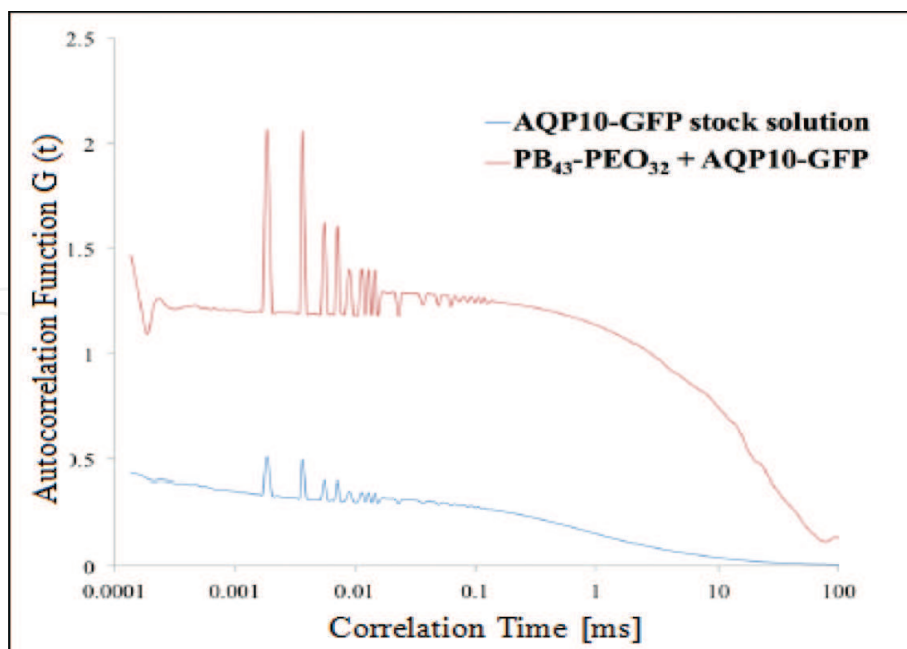


Figure 5. FF-TEM images of PB45-PEO14 proteosomes (b,c,e,f) and polymersomes (a,d). All vesicles showed spots that are potentially not from AqpZ, but instead from the collapsed PB chains (a–c) or failed fracturing phenomena (d–f). Scale bar is 100 nm [86].

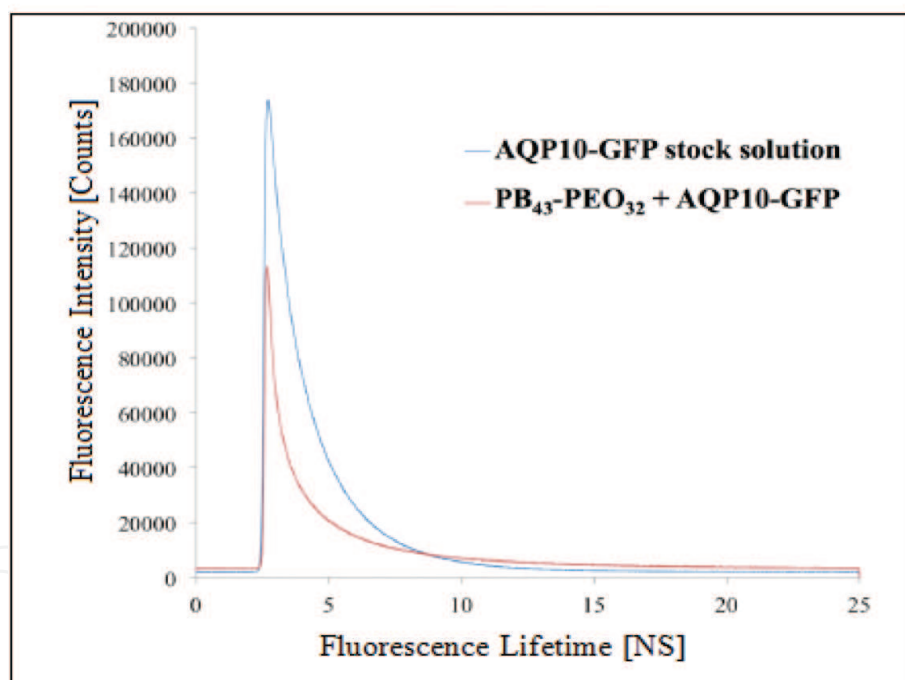
process plays a significant role when it comes to false positive results. Dots were sporadically observed all over the samples, and since these spots were not AqpZ they could be polymer micelles. The observed spots could be removed whenever an augmented concentration step was omitted and the temperature was carefully controlled, after which the sample and cutting handling or metal coating parameters were managed (optimization protocol is provided in the supplementary information section). The existence of AqpZ could not be confirmed, even with polymers that have the shortest PB chains, such as PB45-PEO14 and PB32-PEO30. On the other hand, these experimental runs in themselves cannot reject the potential possibility that AqpZ tetramers could be present, since the hydrophilic PEO chains are comparatively large with respect to lipid head groups. As a consequence, some of the AqpZ may be hidden within the PB core structure.

2.3. Fluorescence correlation spectroscopy

FF-TEM and SFLS can result in several issues when applied as tools for potential evaluation of protein incorporation into polymersomes. As an alternative, FCS was examined as a possible method for collecting relevant quantitative data about the AQP incorporation process. The turn to FCS as a method was motivated by a recent Erbakan *et al.* research study published on the subject. In this paper, Erbakan *et al.* examine a range of AqpZ isoforms that are tagged with fluorophore in proteoliposomes, and where the protein-per-vesicle ratio was calculated and then validated with the help of SFLS [83]. One of the first steps to making this methodology more applicable is attempting to replicate Erbakan *et al.* and their proteoliposome experiments outlined in Ref. [83]. During an experimental run at an mPAR of 1:200, the measurements showed a proteins-per-vesicle-ratio of 5.35, a value comparable to the data found by Erbakan *et al.* at around 7.5. The variance in values could be created by the different AQP and the type of tagged fluorophore applied. Once the FCS instrument values for proteopolymersomes were optimized (further details available in the supporting information), FCS was implemented on the proteopolymersomes of PB45-PEO14 (mPAR 1:100), with AQP10- green fluorescent protein (GFP), and featuring OG-solubilized protein micelles. The data results from this application are outlined in **Figure 6**. In this case, a greater species number was achieved in the proteopolymersomes test sample than in the sample of protein micelle. This discrepancy in species number may be caused by the same type of OG-induced accumulation. Greater autocorrelation signal value suggests a smaller number of particles in the confocal volume because of the slower diffusion time during the process. In this research attempt to simulate results obtained by Erbakan *et al.*, proteopolymersomes were also compared to the AQP10-GFP stock available. Researches Erbakan *et al.* were not able to do such a run, since the fluorophore applied (specifically, mBanana fluorescent protein) displayed a reduced fluorescence lifetime within pure OG environment (stock solution) when matched to the lipid/OG environment of solubilized protein micelles. On the other hand, GFP did not appear to change fluorescence lifetime values substantially even though AQP10-GFP was in OG (1.8 ns) and polymer/OG environmental parameters (1.97 ns, **Figure 6b**). These are similar to fluorophore implemented by Erbakan *et al.* (4 ns [83]) as part of the experiment and to the standardized GFP fluorescence lifetime values (3 ns). The variance in terms of the research project's GFP



(a)



(b)

Figure 6. (a) Correlation diagram of proteopolymerosomes and AQP10-GFP stock solution as a function of correlation time value τ against autocorrelation function $G(\tau)$. (b) Fluorescence lifetimes of the same batch of samples as a function of lifetime against intensity signal. In the instances where the intensities varied, the fluorescence lifetime was in a comparable range [83].

fluorescence lifetime values and the standardized data may be due to the shielding of the attached AQP10 and the OG environment, in addition to the possible influence of the instrument's fitting algorithm.

Research conducted suggests that the example correlation relies on the sole constituent of the system. For instance, when it comes to sensitive fluorophores, it is more important to comparatively analyze the AQP vesicles with the AQP micelles so as to limit the potential impact on the fluorophore environment. With polymers, including the protein matrix, it is more advantageous to relate the AQP-fluorophore stock solution since the polymeric AQP micelles are capable of aggregating more easily. The difficulty caused by the correlation of AQP vesicles with AQP-fluorophore stock is that the resulting concentration value of AQP remains undetermined, and this seriously obscures the potential correlation with analogous AQP concentrations. Based on the species amount of pure AQP10-GFP in the confocal volume stock and the quantity from the proteopolymersome solution (**Figure 6a**), the proteins-per-vesicle-ratio was calculated as 2.87. The data obtained during these experimental runs show that FCS can in fact be applied as a dependable method for calculating AQPs in proteopolymersomes. This in turn invites a new opportunity for conducting a methodical research study where f and M_n are differentiated so as to locate relevant quantitative data about the wide range of polymers that can help obtain the highest proteins-per-vesicle-ratio values.

2.4. Small-angle X-ray scattering

Figure 7 showcases the scattering curves for FR prepared proteo- and polymersomes for PB33-PEO18 and PB45-PEO14. These examples went through a process of extruding and centrifuging before the actual measurements were taken. The typical linear slope was detected at low q values in the log-log plot, and featuring intensity that reflects the $q - 2$ power law. This type of response is characteristic in flat laminar structures. The extension of the slope far below the smallest detectable q -region indicates that there is a low curvature, or flat arrangement, even

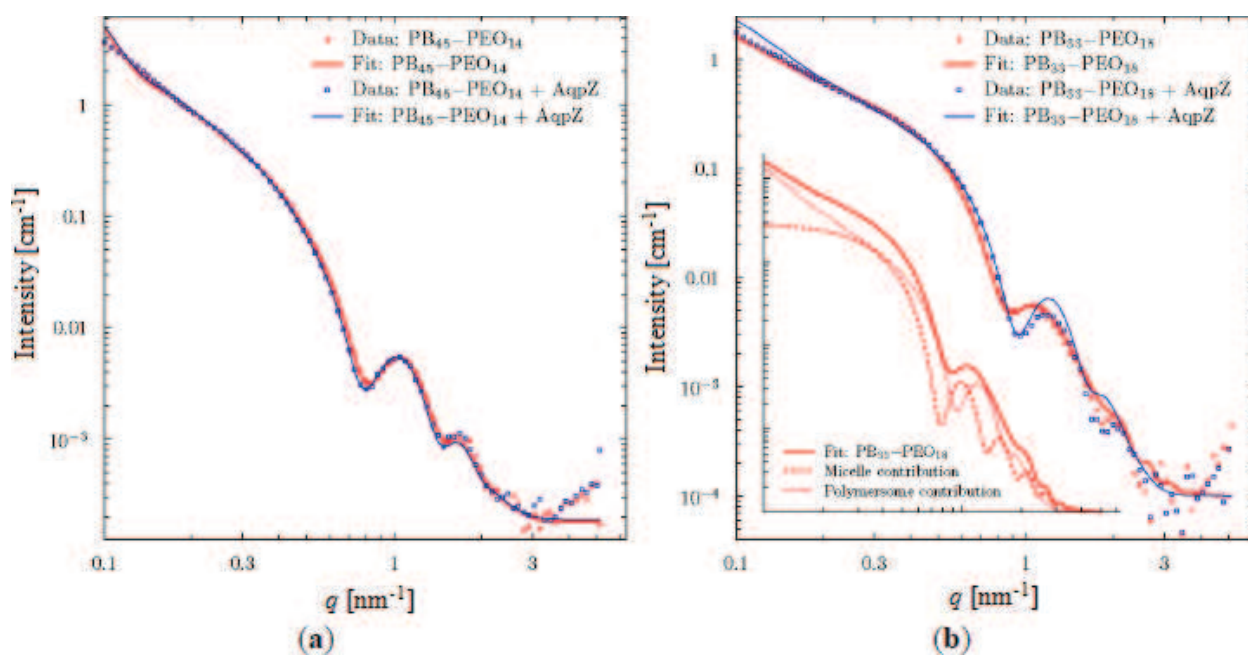


Figure 7. SAXS information for proteo- and polymersomes of (a) PB45-PEO14, and (b) PB33-PEO18 [83].

when it comes to the highest measurable length scale value of $q = 2\pi/0.1 \text{ nm} \approx 60 \text{ nm}^{-1}$. A typical oscillatory behavior occurs at higher q values, and could be caused by the problematic interference happening between positive contrast of PEO and negative contrast of PB. **Figure 7** shows that the fits were acquired with the help of a vesicle model involving three concentric spherical shells. In order to properly fit the PB33-PEO18 polymersomes, an additional contribution from block-copolymer micelles was necessary.

In cases focusing on the theoretical scattering in assorted straightforward geometrical objects, including spheres, ellipsoids, and cylinders of different contrast, the scattering values can be carefully calculated with relative ease. In fact, this data can be collected so as to form simplified models of the particles being studied. In this research model, the data were examined with the aid on a vesicle model based on three concentric spherical shells featuring interchanging contrast values and matched to shells of PEO, PB, and PEO. The thickness values varied in each individual shell so as to ensure the data fit and accuracy through the application of the least squares fitting routine. Exceptionally good fit correlations were found for the PB45-PEO14-system, further suggesting that the research data were in excellent agreement with the theoretical presupposition that diblock copolymers could form spherical vesicle structures. The correlated fits were shown to be especially sensitive to fluctuations in the factors that affect the central hydrophobic bilayer thickness founded using the PB-groups. These values were found to be in the ranges of 9.10 ± 0.1 and $8.94 \pm 0.07 \text{ nm}$ in the cases where AqpZ was either present or absent, respectively. With regards to the overall vesicle diameter value, the model suggests that it is greater than 60 nm , a result that aligns well with the initial analysis of the system. The collected data reflects that the fit parameters defining bilayer vesicles are created and that the inclusion of AqpZ incites very slight changes in the vesicles' structure.

In the case of the PB33-PEO18 proteopolymersomes, sufficiently suitable fits were obtained with the vesicle model based on a hydrophobic bilayer with the thickness values of $7.66 \pm 0.05 \text{ nm}$. On the other hand, for experimental runs with polymersomes, there were no adequate fit options for the data that would ensure realistic physical parameters. In fact, for the data to fit the experimental approach needed to assume that the vesicles could coexist with a population of block copolymer micelles. The combined model fit parameters suggested that 76 wt% of the population was comprised of proteopolymersomes, and that 24 wt% were micelles with hydrophobic cores of diameter $11.7 \pm 0.3 \text{ nm}$, thus showing a relatively good fit with the data overall. The **Figure 7** insert outlines the separate micelle and vesicle contributions.

To sum up, the SAXS inquiry exposes that in the case of for PB45-PEO14 the vesicles are created both with, as well as without, the AQP, where the AQP incorporation leads to a small variance in the average hydrophobic vesicle wall thickness value, and can imply a polymer puckering and dimpling near the integrated AQPs. For the PB33-PEO18 experimental runs, some micelle creation was seen, but this formation becomes lower once the AQP is successfully integrated. To sum up, this chapter examines the research that explored the characterization methods used for the functional integration of AQPs in PB-PEO diblock copolymers. The research results obtained suggest that both FF-TEM and

SFLS are in theory effective methods, however, when it comes to polymer systems the critical analysis of findings can provide ambiguous data that makes it problematic for applications. Alternatively, SAXS and FCS have been evaluated as capable of producing relevant information, with SAXS relying on access to large-scale facilities that can sustain synchrotron radiation resources.

Author details

Amira Abdelrasoul^{1*}, Huu Doan² and Ali Lohi²

*Address all correspondence to: amira.abdelrasoul@usask.ca

1 Department of Chemical and Biological Engineering, University of Saskatchewan, Saskatoon, Saskatchewan, Canada

2 Department of Chemical Engineering, Ryerson University, Toronto, Ontario, Canada

References

- [1] Kagawa Y, Racker E. Partial resolution of the enzymes catalyzing oxidative phosphorylation. *The Journal of Biological Chemistry*. 1971;**246**:5477-5487
- [2] Nardin C, Thoeni S, Widmer J, Winterhalter M, Meier W. Nanoreactors based on (polymerized) ABA-triblock copolymer vesicles. *Chemical Communications*. 2000:1433-1434
- [3] Zhang X, Tanner P, Graff A, Palivan CG, Meier W. Mimicking the cell membrane with block copolymer membranes. *Journal of Polymer Science, Part A: Polymer Chemistry*. 2012;**50**:2293-2318
- [4] Tanner P, Baumann P, Enea R, Onaca O, Palivan C, Meier W. Polymeric vesicles: From drug carriers to nanoreactors and artificial organelles. *Accounts of Chemical Research*. 2011;**44**:1039-1049
- [5] Choi HJ, Montemagno C. Artificial organelle: ATP synthesis from cellular mimetic polymersomes. *Nano Letters*. 2005;**5**:2538-2542
- [6] VriezemaDM, GarciaPML, SanchoOltraN, HatzakisNS, KuiperSM, NolteRJM, RowanAE, van Hest JCM. Positional assembly of enzymes in polymersome nanoreactors for cascade reactions. *Angewandte Chemie, International Edition*. 2007;**46**:7378-7382
- [7] Kumar M, Grzelakowski M, Zilles J, Meier WP. Highly permeable polymeric membranes based on the incorporation of the functional water channel protein aquaporin Z. *Proceedings of the National Academy of Sciences of the United States of America*. 2007;**104**:20719-20724

- [8] Kumar M, Habel J, Shen YX, Meier W, Walz T. High-density reconstitution of functional water channels into vesicular and planar block copolymer membranes. *Journal of the American Chemical Society*. 2012;**134**:18631-18637
- [9] Andersen O. Bilayer thickness and membrane protein function: An energetic perspective. *Annual Review of Biophysics and Biomolecular Structure*. 2007;**36**:107-130
- [10] Pata V, Dan N. The effect of chain length on protein solubilization in polymer-based vesicles (polymersomes). *Biophysical Journal*. 2003;**85**:2111-2118
- [11] Srinivas G, Discher D, Klein M. Key roles for chain flexibility in block copolymer membranes that contain pores or make tubes. *Nano Letters*. 2005;**5**:2343-2349
- [12] Discher DE, Ortiz V, Srinivas G, Klein ML, Kim Y, Christian D, Cai S, Photos P, Ahmed F. Emerging applications of polymersomes in delivery: From molecular dynamics to shrinkage of tumors. *Progress in Polymer Science*. 2007;**32**:838-857
- [13] Aponte-Santamaría C, Briones R, Schenk A, Walz T, de Groot B. Molecular driving forces defining lipid positions around aquaporin-0. *Proceedings of the National Academy of Sciences of the United States of America*. 2012;**109**:9887-9892
- [14] Hansen JS, Vararattanavech A, Plasencia I, Greisen PJ, Bomholt J, Torres J, Emnéus J, Hélix-Nielsen C. Interaction between sodium dodecyl sulfate and membrane reconstituted aquaporins: A comparative study of spinach SoPIP2;1 and *E. coli* AqpZ. *Biochimica et Biophysica Acta (BBA) - Biomembranes*. 2011;**1808**:2600-2607
- [15] Stoenescu R, Graff A, Meier W. Asymmetric ABC-triblock copolymer membranes induce a directed insertion of membrane proteins. *Macromolecular Bioscience*. 2004;**4**:930-935
- [16] Hite RK, Li Z, Walz T. Principles of membrane protein interactions with annular lipids deduced from aquaporin-0 2D crystals. *The EMBO Journal*. 2010;**29**:1652-1658
- [17] Nehring R, Palivan CG, Casse O, Tanner P, Tüxen J, Meier W. Amphiphilic diblock copolymers for molecular recognition: Metal-nitrilotriacetic acid functionalized vesicles. *Langmuir*. 2009;**25**:1122-1130
- [18] Kelly D, Abeyrathne P, Dukovski D. The affinity grid: A pre-fabricated EM grid for monolayer purification. *Journal of Molecular Biology*. 2008;**382**:423-433
- [19] Kumar M. Biomimetic membranes as new materials for applications in environmental engineering and biology. Ph.D. Thesis. Champaign, IL, USA: University Illinois; 2010
- [20] Kumar M, Meier W. Highly Permeable Polymeric Membranes. Patent WO 2009/078174; 18-06-2009
- [21] Gonen T, Sliz P, Kistler J, Cheng Y, Walz T. Aquaporin-0 membrane junctions reveal the structure of a closed water pore. *Nature*. 2004;**429**:193-197
- [22] Chandy G, Zampighi G, Kreman M, Hall J. Comparison of the water transporting properties of MIP and AQP1. *The Journal of Membrane Biology*. 1997;**159**:29-39

- [23] Kumar M, Walz T. High Density Membrane Protein Membranes. Patent WO 2014/028923; 20-02-2014
- [24] Habel J. Structural and functional characterization of aquaporin 0 incorporated in block copolymers and their resulting aggregate morphologies. Master Thesis. Basel, Switzerland: Universität Basel; 2011
- [25] Hélix-Nielsen C. Biomimetic membranes for sensor and separation applications. *Analytical and Bioanalytical Chemistry*. 2009;**395**:697-718
- [26] Pszon-Bartosz K, Hansen JS, Stibius KB, Groth JS, Emnéus J, Geschke O, Hélix-Nielsen C. Assessing the efficacy of vesicle fusion with planar membrane arrays using a mitochondrial porin as reporter. *Biochemical and Biophysical Research Communications*. 2011;**406**:96-100
- [27] González-Pérez A, Stibius K, Vissing T. Biomimetic triblock copolymer membrane arrays: A stable template for functional membrane proteins. *Langmuir*. 2009;**25**:10447-10450
- [28] Graff A. Amphiphilic copolymer membranes promote NADH: Ubiquinone oxidoreductase activity: Towards an electron-transfer nanodevice. *Macromolecular Chemistry and Physics*. 2010;**211**:229-238
- [29] Wong D, Jeon TJ, Schmidt J. Single molecule measurements of channel proteins incorporated into biomimetic polymer membranes. *Nanotechnology*. 2006;**17**:3710-3717
- [30] Uehlein N, Otto B, Eilingsfeld A, Itel F, Meier W, Kaldenhoff R. Gas-tight triblock-copolymer membranes are converted to CO₂ permeable by insertion of plant aquaporins. *Scientific Reports*. 2012;**2**:1-4
- [31] Wang H, Chung TS, Tong YW. Study on water transport through a mechanically robust aquaporin Z biomimetic membrane. *Journal of Membrane Science*. 2013;**445**:47-52
- [32] Wang H, Chung TS, Tong YW, Jeyaseelan K, Armugam A, Chen Z, Hong M, Meier W. Highly permeable and selective pore-spanning biomimetic membrane embedded with aquaporin Z. *Small*. 2012;**8**:1185-1190
- [33] Zhong PS, Chung TS, Jeyaseelan K, Armugam A. Aquaporin-embedded biomimetic membranes for nanofiltration. *Journal of Membrane Science*. 2012;**407-408**:27-33
- [34] De Vocht C, Ranquin A, Willaert R, Van Ginderachter JA, Vanhaecke T, Rogiers V, Versées W, Van Gelder P, Steyaert J. Assessment of stability, toxicity and immunogenicity of new polymeric nanoreactors for use in enzyme replacement therapy of MNGIE. *Journal of Controlled Release*. 2009;**137**:246-254
- [35] Grzelakowski M, Cherenet MF, Shen YX, Kumar M. A framework for accurate evaluation of the promise of aquaporin based biomimetic membranes. *Journal of Membrane Science*. 2015:1-32
- [36] Grzelakowski M, Onaca O, Rigler P, Kumar M, Meier W. Immobilized protein-polymer nanoreactors. *Small*. 2009;**5**:2545-2548

- [37] Ihle S, Onaca O, Rigler P, Hauer B, Rodríguez-Ropero F, Fioroni M, Schwaneberg U. Nanocompartments with a pH release system based on an engineered OmpF channel protein. *Soft Matter*. 2011;**7**:532-539
- [38] Tanner P, Balasubramanian V, Palivan CG. Aiding nature's organelles: Artificial peroxisomes play their role. *Nano Letters*. 2013;**13**:2875-2883
- [39] Tanner P, Onaca O, Balasubramanian V, Meier W, Palivan CG. Enzymatic cascade reactions inside polymeric nanocontainers: A means to combat oxidative stress. *Chemistry - A European Journal*. 2011;**17**:4552-4560
- [40] Kowal JL, Kowal JK, Wu D, Stahlberg H, Palivan CG, Meier WP. Functional surface engineering by nucleotide-modulated potassium channel insertion into polymer membranes attached to solid supports. *Biomaterials*. 2014;**35**:7286-7294
- [41] Winterhalter M, Hilty C, Bezrukov SM, Nardin C, Meier W, Fournier D. Controlling membrane permeability with bacterial porins: Application to encapsulated enzymes. *Talanta*. 2001;**55**:965-971
- [42] Xie W, He F, Wang B, Chung TS, Jeyaseelan K, Armugam A, Tong YW. An aquaporin-based vesicle-embedded polymeric membrane for low energy water filtration. *Journal of Materials Chemistry A*. 2013;**1**:7592-7600
- [43] Heinisch T, Langowska K, Tanner P, Reymond JL, Meier W, Palivan C, Ward TR. Fluorescence-based assay for the optimization of the activity of artificial transfer hydrogenase within a biocompatible compartment. *ChemCatChem*. 2013;**5**:720-723
- [44] Broz P, Driamov S, Ziegler J, Ben-Haim N, Marsch S, Meier W, Hunziker P. Toward intelligent nanosize bioreactors: A pH-switchable, channel-equipped, functional polymer nanocontainer. *Nano Letters*. 2006;**6**:2349-2353
- [45] Langowska K, Palivan CG, Meier W. Polymer nanoreactors shown to produce and release antibiotics locally. *Chemical Communications*. 2013;**49**:128-130
- [46] Graff A, Sauer M, Meier W. Virus-assisted loading of polymer nanocontainer. *Proceedings of the National Academy of Sciences of the United States of America*. 2002;**99**:5064-5068
- [47] Ranquin A, Versées W, Meier W, Steyaert J, Van Gelder P. Therapeutic nanoreactors: Combining chemistry and biology in a novel triblock copolymer drug delivery system. *Nano Letters*. 2005;**5**:2220-2224
- [48] Lee H, Ho D, Kuo K, Montemagno CD. Vectorial insertion of bacteriorhodopsin for directed orientation assays in various polymeric biomembranes. *Polymer*. 2006;**47**:2935-2941
- [49] Choi HJ, Germain J. Effects of different reconstitution procedures on membrane protein activities in proteopolymersomes. *Nanotechnology*. 2006;**17**:1825-1830
- [50] Choi HJ, Montemagno CD. Biosynthesis within a bubble architecture. *Nanotechnology*. 2006;**17**:2198-2202

- [51] Choi HJ, Montemagno C. Light-driven hybrid bioreactor based on protein-incorporated polymer vesicles. *IEEE Transactions on Nanotechnology*. 2007;**6**:171-176
- [52] Dobrunz D, Toma AC, Tanner P, Pfohl T, Palivan CG. Polymer Nanoreactors with dual functionality: Simultaneous detoxification of peroxyxynitrite and oxygen transport. *Langmuir*. 2012;**28**:15889-15899
- [53] Thoma J, Belegriou S, Roszbach P, Grzelakowski M, Kita-Tokarczyk K, Meier W. Membrane protein distribution in composite polymer-lipid thin films. *Chemical Communications*. 2012;**48**:8811-8813
- [54] Onaca O, Sarkar P, Roccatano D, Friedrich T, Hauer B, Grzelakowski M, Güven A, Fioroni M, Schwaneberg U. Functionalized nanocompartments (synthosomes) with a reduction-triggered release system. *Angewandte Chemie, International Edition*. 2008;**47**:7029-7031
- [55] Ho D, Chu B, Lee H, Montemagno C. Protein-driven energy transduction across polymeric biomembranes. *Nanotechnology*. 2004. DOI: 10.1088/0957-4484/15/8/038
- [56] Ho D, Chu B, Lee H, Brooks EK, Kuo K, Montemagno CD. Fabrication of biomolecule-copolymer hybrid nanovesicles as energy conversion systems. *Nanotechnology*. 2005;**16**:3120-3132
- [57] Xi JZ, Ho D, Chu B, Montemagno CD. Lessons learned from engineering biologically active hybrid nano/micro devices. *Advanced Functional Materials*. 2005;**15**:1233-1240
- [58] Ho D, Chu B, Schmidt JJ, Brooks EK, Montemagno CD. Hybrid protein-polymer biomimetic membranes. *IEEE Transactions on Nanotechnology*. 2004;**3**:256-263
- [59] Habel J. Functional and Chemical Characterization of Vesicular Diblock Copolymer Bilayers with Aquaporin Included. Technical Report, Aquaporin A/S, Copenhagen, Denmark; 2011
- [60] Espina M. Barrier properties of biomimetic membranes. Master Thesis. Lyngby, Denmark: Danish Technical University (DTU) Kgs; 2012
- [61] Nallani M, Andreasson-Ochsner M, Tan CWD, Sinner EK, Wisantoso Y, Geifman-Shochat S, Hunziker W. Proteopolymersomes: *In vitro* production of a membrane protein in polymersome membranes. *Biointerfaces*. 2011;**6**:153-157
- [62] Bomholt J. Human Aquaporins—From *in vivo* detection to industrial scale production. Ph.D. Thesis. Copenhagen, Denmark: University Copenhagen; 2014
- [63] Onaca O. Functionalized polymer vesicles and interactions with Polymyxin B and derivatives. Ph.D. Thesis. Bremen, Germany: Universität Bremen; 2007
- [64] Zhang X, Fu W, Palivan CG, Meier W. Natural channel protein inserts and functions in a completely artificial, solid-supported bilayer membrane. *Scientific Reports*. 2013;**3**. DOI: 10.1038/srep02196
- [65] Dorn J, Belegriou S, Kreiter M, Sinner EK, Meier W. Planar block copolymer membranes by vesicle spreading. *Macromolecular Bioscience*. 2011;**11**:514-525

- [66] Vijayan K, Discher DE, Lal J, Janmey P, Goulian M. Interactions of membrane-active peptides with thick, neutral, nonzwitterionic bilayers. *The Journal of Physical Chemistry. B.* 2005;**109**:14356-14364
- [67] Toughrai S. Functional surfaces through biomimetic block copolymer membranes. Ph.D. Thesis. Basel, Switzerland: Universität Basel; 2014
- [68] Amado E, Schöps R, Brandt W, Kressler J. Spontaneous formation of giant bioactive protein-block copolymer vesicles in water. *ACS Macro Letters.* 2012;**1**:1016-1019
- [69] Noor M, Dworeck T, Schenk A, Shinde P, Fioroni M, Schwaneberg U. Polymersome surface decoration by an EGFP fusion protein employing Cecropin a as peptide "anchor". *Journal of Biotechnology.* 2012;**157**:31-37
- [70] Kuang L, Fernandes DA, O'Halloran M, Zheng W, Jiang Y, Ladizhansky V, Brown LS, Liang H. "Frozen" block copolymer nanomembranes with light-driven proton pumping performance. *ACS Nano.* 2014;**8**:537-545
- [71] Hua D, Kuang L, Liang H. Self-directed reconstitution of proteorhodopsin with amphiphilic block copolymers induces the formation of hierarchically ordered proteopolymer membrane arrays. *Journal of the American Chemical Society.* 2011;**133**:2354-2357
- [72] Kuang L, Olson TL, Lin S, Flores M, Jiang Y, Zheng W, Williams JC, Allen JP, Liang H. Interface for light-driven electron transfer by photosynthetic complexes across block copolymer membranes. *Journal of Physical Chemistry Letters.* 2014;**5**:787-791
- [73] Andreasson-Ochsner M, Fu Z, May S, Ying Xiu L, Nallani M, Sinner EK. Selective deposition and self-assembly of triblock copolymers into matrix arrays for membrane protein production. *Langmuir.* 2012;**28**:2044-2048
- [74] Gulati S, Jamshad M, Knowles TJ, Morrison KA, Downing R, Cant N, Collins R, Koenderink JB, Ford RC, Overduin M, et al. Detergent-free purification of ABC (ATPbinding-cassette) transporters. *The Biochemical Journal.* 2014;**461**:269-278
- [75] Knowles TJ, Finka R, Smith C, Lin YP, Dafforn T, Overduin M. Membrane proteins solubilized intact in lipid containing nanoparticles bounded by styrene maleic acid copolymer. *Journal of the American Chemical Society.* 2009;**131**:7484-7485
- [76] Hall AR, Scott A, Rotem D, Mehta KK, Bayley H, Dekker C. Hybrid pore formation by directed insertion of α -haemolysin into solid-state nanopores. *Nature Nanotechnology.* 2010;**5**:874-877
- [77] Balme S, Janot JM, Berardo L, Henn F, Bonhenry D, Kraszewski S, Picaud F, Ramseyer C. New bioinspired membrane made of a biological ion channel confined into the cylindrical nanopore of a solid-state polymer. *Nano Letters.* 2011;**11**:712-716
- [78] Ibragimova S. Supporting and stabilizing biomimetic membranes. Ph.D. Thesis. Lyngby, Denmark: Danish Technical University, Kgs; 2011
- [79] Mech-Dorosz A, Heiskanen A, Bäckström S, Perry M, Muhammad HB, Hélix-Nielsen C, Emnéus J. A reusable device for electrochemical applications of hydrogel supported black lipid membranes. *Biomedical Microdevices.* 2015;**17**:21

- [80] Bodor S, Zook JM, Lindner E, Tóth K, Gyurcsányi RE. Electrochemical methods for the determination of the diffusion coefficient of ionophores and ionophore-ion complexes in plasticized PVC membranes. *Analyst*. 2008;**133**:635-642
- [81] Discher DE. Polymer vesicles. *Science*. 2002;**297**:967-973
- [82] Nardin C, Hirt T, Leukel J, Meier W. Polymerized ABA triblock copolymer vesicles. *Langmuir*. 2000;**16**:1035-1041
- [83] Erbakan M, Shen YX, Grzelakowski M, Butler PJ, Kumar M, Curtis WR. Molecular cloning, overexpression and characterization of a novel water channel protein from rhodospirillum rubrum. *PLoS One*. 2014;**9**:e86830
- [84] Ibata K, Takimoto S, Morisaku T, Miyawaki A, Yasui M. Analysis of aquaporin-mediated diffusional water permeability by coherent anti-stokes raman scattering microscopy. *Biophysical Journal*. 2011;**101**:2277-2283
- [85] Mamonov AB, Coalson RD, Zeidel ML, Mathai JC. Water and deuterium oxide permeability through aquaporin 1: MD predictions and experimental verification. *The Journal of General Physiology*. 2007;**130**:111-116
- [86] Itel F, Al-Samir S, Oberg F, Chami M, Kumar M, Supuran CT, Deen PMT, Meier W, Hedfalk K, Gros G, Endeward V. CO₂ permeability of cell membranes is regulated by membrane cholesterol and protein gas channels. *The FASEB Journal*. 2012;**26**:5182-5191

